J. Fluid Mech. (1983), *vol.* 128, *pp.* 259–282
Printed in Great Britain

The dynamics of double-diffusive gravity currents

By T. MAXWORTHY

Departments of Mechanical and Aerospace Engineering, University of Southern California, Los Angeles, CA 90089

(Received 11 June 1982 and in revised form 23 August 1982)

Gravity currents or intrusions for which the fluid within the current contains a substance that gives it a diffusivity different from that of its surroundings are very common both in natural and technological applications. The interface between the two fluids can become the site of either a 'fingering' or a 'diffusive' type of instability, and vigorous convection and material exchange occurs (Turner 1975). This transfer of material has several important effects upon the dynamics of the intrusion. Horizontal momentum can be transferred across the interface to create a stress which in many cases dominates the more conventional viscous stresses. Entrainment into the convective plume beneath the intrusion and, in a container of finite depth, the formation of a secondary, bottom-boundary current, creates a flow external to the main intrusion which modifies its behaviour even more. Two cases have been studied: the release of a fixed volume of fluid and the injection of fluid at a constant rate for both types of interface. Several experiments on the motion of an intrusion for which the interface is essentially non-diffusive are presented for comparison.

1. Introduction

When light fluid is introduced into a body of denser fluid, it spreads at the surface in a predictable way if the characteristic substance (e.g. heat, a dissolved solute) that gives the fluids their density difference is the same (Hoult 1972; Simpson 1982; Turner 1974; Didden & Maxworthy 1982; Maxworthy 1983; Huppert 1982). It is also well known that, when the two fluids have a density difference due to substances of different diffusivities, the interface between them can become the site of a double-diffusive instability even if the overall density difference is stable. The literature on this latter subject, when the two fluids are not in relative horizontal motion in the mean, is particularly rich, and has been reviewed in detail by Turner (1973, 1974) and Huppert & Turner (1981). In only a few cases have the two problems been combined to study the effects of these double-diffusive processes on the motion of the intruding fluid (Turner 1978; Ruddick & Turner 1979) or the effect of interfacial shear on the magnitude of the fluxes across the interface (Linden 1974). In what follows, we present experiments aimed at gaining a basic understanding of such a system in the simplest possible circumstance: that of the intrusion of a sugar or salt solution into an ambient fluid made denser by the addition of salt or sugar respectively.

It has become standard to use sugar and salt solutions in order to run experiments on double-diffusive effects because, as is required, the diffusivity of one (sugar) is smaller than that of the other (salt). These then serve as models for one pair of naturally occurring substances of major interest, salt and heat, for which the diffusivity ratio is large, of order 100 compared to three for the salt/sugar system.

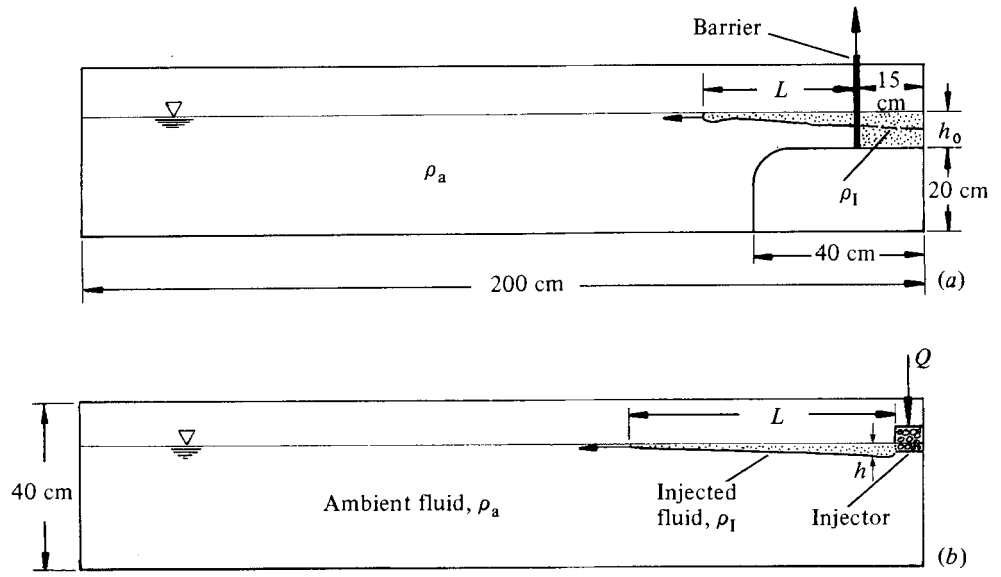

FIGURE 1. (*a*) Apparatus for a surface gravity current or intrusion with a constant inflow rate. The ambient fluid was either a salt solution or a sugar solution of density ρ_a, in which case the fluid (ρ_1) released from behind the moveable barrier was either a sugar or salt solution respectively. (*b*) Same tank as (*a*), but with an injector inserted so that a fixed flow rate could be released into the ambient fluid.

The works of Stern & Turner (1969), Turner (1975) and Shirtcliffe (1973), among others, have shown that the basic double-diffusive properties of such systems are qualitatively similar, although actual flux ratios and rates do depend on the diffusivity ratio. For experimental convenience we use the sugar/salt combination in what follows.

We also present two theoretical models which we believe help clarify the role of these phenomena in two cases, the release of a constant volume and the injection of a constant flux of lighter fluid. In both cases the experiments tend to support the models to some extent, although several effects, which while not measured directly were observed qualitatively, cloud the issue and require more detailed study in the future.

Double-diffusive phenomena have important applications in both natural systems, for example in the study of the dynamics of intrusions in the oceans and atmosphere, and in technology, where problems involving the motion of liquid natural-gas spills (Turner, private communication) and of sewage and waste water disposal (Fischer 1971) have been thought to involve them. Thus a good understanding of such effects is desirable if we wish to say we truly understand the overall problem of their influence on the natural environment.

2. Apparatus

The apparatus used in these experiments was similar to that used in Didden & Maxworthy (1982 hereinafter referred to as DM), although it is different in some details. The test tank was smaller, being 2 m long, 40 cm deep and 15 cm wide (see figure 1), and was constructed of plate glass to facilitate observation of the density field by a shadowgraph technique.

Two types of fluid release were used. The first, which had no counterpart in the experiments of DM, consisted of a dammed section at one end of the tank from which a fixed volume of light fluid could be released (figure 1*a*). The second consisted of a plenum chamber and slit connected to a flow meter and fluid reservoir in order to produce a uniform inflow of constant flow rate (figure 1*b*), as in DM.

We have run a variety of experiments with each of these configurations, including a series with fixed initial fluid volume, but with different values of initial depth h_0 and density ratio (see below), and a series with fixed initial flow rates $\tilde{q}$. In each series of experiments three different interface types were considered: (i) an essentially non-diffusive interface, i.e. brine solution intruding into a brine solution of higher density; (ii) an interface unstable to a 'salt-fingering' instability produced by introducing a sugar solution over a heavier brine solution; and (iii) a 'diffusive interface' that is a sharp convecting transition zone produced by running a salt solution over a sugar solution.

The important density ratios used here include $\Delta\rho/\rho_a$, where $\Delta\rho = \rho_a - \rho_I$ (see figure 1), and the ratio of the contributions of the two components to the density difference across the interface; $\beta\Delta S/\alpha\Delta T \equiv R_\rho$ for the 'diffusive' case and $\alpha\Delta T/\beta\Delta S \equiv R'_\rho$ for the 'fingering' interface, using the accepted nomenclature for each of these quantities. Here the density of the faster-diffusing solution (brine) is $\rho_0(1+\alpha\Delta T)$, and that of the slower-diffusing substance (sugar) $\rho_0(1+\beta\Delta S)$, where ρ_0 is the density of the pure solvent, in this case water. Both R_ρ and R'_ρ vary between unity and infinity, with the most vigorous convection taking place when the ratio is close to unity.

In all cases the length of the gravity current was measured as a function of time by placing both a lengthscale and a clock in the field of view of a fixed 35 mm camera fitted with a lens of long focal length.

3. Theoretical preliminaries

3.1. *Plane, diffusive or fingering gravity currents*

Here we anticipate, to some extent, the results to be presented in the following sections and discuss a series of models that appear to have some relevance to the experimental results. We start by noting that, owing to the strong double-diffusive instability that occurs, net amounts of material and horizontal momentum are transferred across the interface between the two fluids. This we show diagrammatically in figure 2, where V is a measure of the vertical velocity across the interface due to the instability,† U is a representative velocity within the intrusion itself and is taken equal to L/t (see figure 1), and U_∞ is the velocity external to the intrusion caused, for example, by entrainment into the external plume of unstable material, as will be explained in §4. Also, as will be shown in §5, V can be estimated from the flux laws measured by Shirtcliffe (1973) and Griffiths & Ruddick (1980), assuming that the quasi-steady-state results reported there hold in this case.

As has been shown in DM in all experimental laboratory-scale results to date, the so-called 'bottom or solid boundary current' is the one that is found, because even a nominally free surface acts as a solid boundary owing to contained impurities. In the present notation the magnitude for the 'bottom' force per unit width acting along the whole length of the current is $F_B \propto \mu UL/h$, where μ is the coefficient of viscosity

† Since the characteristic upward velocity V_U and the downward velocity V_D are of the same order of magnitude, we use the general designation V to represent them in the order-of-magnitude analyses that follow.

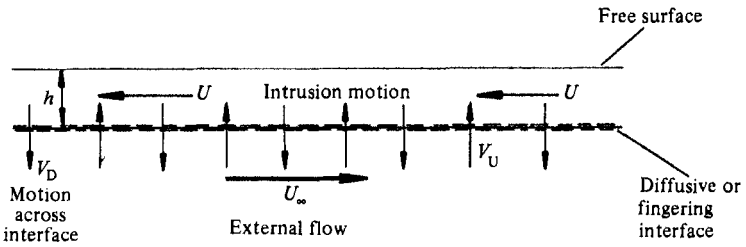

FIGURE 2. Model of the interface between the intruding fluid moving with velocity U and the external fluid moving with velocity U_∞. The instability of the interface causes an interchange of fluid between the two, characterized by averaged vertical velocities V_D and V_U.

and h a representative thickness of the self-similar intrusion. We can now distinguish two extreme cases.

3.1.1. *Intrusion or (U)-dominated case.* Firstly, we assume that U_∞ is small, so that the loss of horizontal momentum from the intrusion itself dominates. Owing to this transfer of momentum the interface is subject to a horizontal force/unit width

$$F_{DD} \propto \rho UVL, \tag{4}$$

so that $F_{DD}/F_B \equiv \mathscr{F} \propto VH/\nu$, where $\nu = \mu/\rho$ is the kinematic viscosity.

As in Huppert (1982) and Maxworthy (1982), it is now convenient to consider a fairly general release-rate relationship, in order to cover as wide a range of cases as possible, such that the intrusion volume per unit width of the channel varies as the power of the time:

$$Lh \propto \tilde{q}t^\alpha. \tag{5}$$

Hence

$$\mathscr{F} \propto \frac{V\tilde{q}t^\alpha}{\nu L}.$$

If we assume that initially the motion $L(t)$ is governed by the relationship for a buoyancy–viscous balance presented in Huppert (1982) and verified experimentally in DM and Maxworthy (1982), i.e.

$$L = k_v \left\{\frac{g'\tilde{q}^3}{\nu}\right\}^{\frac{1}{5}} t^{(3\alpha+1)/5} \tag{6}$$

where $g' = g\,\Delta\rho/\rho$ and g is the acceleration due to gravity. Substituting (6) into the expression for $\mathscr{F}$ leads to an estimate for the transition time t_{TR} at which the interfacial stress becomes important:

$$t_{TR} = C_\alpha \frac{\nu^4 g'}{V^5 \tilde{q}^2}, \tag{7a}$$

where C_α is assumed to be of order unity.

An equivalent and somewhat more revealing expression for t_{TR} can be found by first deriving the needed expression for the evolution of a double-diffusive gravity current by equating the buoyancy force/unit width, from DM,

$$F_g \propto \Delta\rho g h^2, \tag{8}$$

to the interfacial force/unit width, (4), only, assuming that the bottom force is negligibly small, i.e. that $t \gg t_{TR}$. Using (5) it can then be shown that†

$$L = k_\alpha \left\{\frac{g'\tilde{q}^2}{V}\right\}^{\frac{1}{4}} t^{(2\alpha+1)/4} \tag{9}$$

† The axisymmetric case can be treated in a similar manner, and the results are given in the appendix.

At $t = t_{\mathrm{TR}}$, (6) and (9) must be identical so that an alternative to (7*a*) can be derived:

$$t_{\mathrm{TR}} = \left\{\frac{k_\alpha}{k_v}\right\}^{20/(2\alpha-1)} \left\{\frac{\nu^4 g'}{V^5 \tilde{q}^2}\right\}^{1/(2\alpha-1)} \tag{7b}$$

Thus, in a manner entirely equivalent to the discussion of inertial–buoyancy to viscous–buoyancy transitions found in Huppert (1982) and Maxworthy (1982), we find a critical value for α of $\frac{1}{2}$ in this case. This suggests that for $\alpha > \frac{1}{2}$, which includes our present case of constant flow rate ($\alpha = 1$), the transition will be from a viscously controlled to double-diffusively controlled current. While for $\alpha < \frac{1}{2}$ our case of a constant volume release ($\alpha = 0$) is included here, the opposite should occur. However, we will show that other effects dominate before this latter possibility can be realized and so we can make no comment on this interesting question yet.

3.1.2. *Evolution dominated by the outer flow* (U_∞). The second case assumes that the interfacial stress is dominated by the transfer of horizontal momentum from the ambient fluid, moving with velocity U_∞ (figure 2), into the intrusion, and that the stress due to the slug motion itself can be ignored. Now the force balance becomes

$$\Delta\rho g h^2 \approx \rho U_\infty V L,$$

so that the spreading relationship becomes

$$L = k'_\alpha \left\{\frac{g' q^2}{U_\infty V}\right\}^{\frac{1}{3}} t^{2\alpha/3}, \tag{10}$$

and the transition time is given by

$$t'_{\mathrm{TR}} = C'_\alpha \left\{\frac{\nu^3 g'^2 \tilde{q}}{U_\infty^5 V^5}\right\}^{1/(3-\alpha)}, \quad \text{where} \quad C'_\alpha = \left\{\frac{k'_\alpha}{k_v}\right\}^{15/(3-\alpha)}. \tag{11}$$

In this case we find a critical condition at $\alpha = 3$, with transition from a viscously to a double-diffusively controlled current occurring when $\alpha < 3$. This does not exhaust all of the possible transitions, since it is also reasonable to expect that under some conditions a flow initially dominated by momentum transfer from the slug itself will become dominated by transfer from the ambient fluid.† Under these circumstances, the transition time is given by

$$\left\{\frac{k'_\alpha}{k_\alpha}\right\}^{12/(3-2\alpha)} \left\{\frac{g' q^2}{V U_\infty^4}\right\}^{1/(3-2\alpha)}, \tag{12}$$

	Current dominated by U		Current dominated by U_∞	
	L	t_{TR}	L	t_{TR}
$\alpha = 1$	$k_1 \left\{\frac{g' \tilde{q}^2}{V}\right\}^{\frac{1}{4}} t^{\frac{3}{4}}$ (13)	$\left\{\frac{k_1}{k_v}\right\}^{20} \frac{\nu^4 g'}{V^5 \tilde{q}^2}$ (14)	$k'_1 \left\{\frac{g' \tilde{q}^2}{U_\infty V}\right\}^{\frac{1}{3}} t^{\frac{2}{3}}$ (15)	$\left\{\frac{k'_1}{k_v}\right\}^{\frac{15}{2}} \left\{\frac{\nu^3 q'^2 \tilde{q}}{U_\infty^5 V^5}\right\}^{\frac{1}{2}}$ (16)
$\alpha = 0$	$k_0 \left\{\frac{g' q^2}{V}\right\}^{\frac{1}{4}} t^{\frac{1}{4}}$ (17)	$\left\{\frac{k_v}{k_0}\right\}^{20} \frac{V^5 q^2}{\nu^4 g'}$ (18)	$k'_0 \left\{\frac{g' q^2}{U_\infty V}\right\}^{\frac{1}{3}} = \text{const}$ (19)	$\left\{\frac{k'_0}{k_v}\right\}^{\frac{15}{3}} \left\{\frac{\nu^3 g'^2 \tilde{q}}{U_\infty^5 V^5}\right\}^{\frac{1}{3}}$ (20)

TABLE 1

† We will call this a U-to-U_∞ transition in what follows.

with a critical value of α of $\frac{3}{2}$. In this development we have deliberately ignored the possibility of direct transitions from a state of inertia–buoyancy balance, but it should be realized that three more transition times can be derived to account for such possibilities! Fortunately these do not appear to play a role in the experiments to be described, and will not be written down formally or discussed except briefly in the case discussed in §3.2.

As a summary, we present in table 1 the equations that will be of use in interpreting the experimental results and to which must be added the U-to-U_∞ transition time for the case $\alpha = 1$:

$$\left\{\frac{k_1'}{k_1}\right\}^{12}\left\{\frac{g'q^2}{VU_\infty^4}\right\}. \tag{21}$$

3.2. *Plane non-diffusive gravity current*

In the experiments to be described, we contrast the behaviour of the double-diffusively controlled current with that for which the viscous bottom force is the only retarding force. For these latter cases, Huppert (1982) gives, from (6), for $\alpha = 1$

$$L = k_1''\left\{\frac{g'\tilde{q}^3}{\nu}\right\}^{\frac{1}{5}} t^{\frac{4}{5}}, \tag{22}$$

a result that has been confirmed experimentally in DM and Maxworthy (1982), while for $\alpha = 0$

$$L = k_0''\left\{\frac{g'\tilde{q}^3}{\nu}\right\}^{\frac{1}{5}} t^{\frac{1}{5}}. \tag{23}$$

In this latter case, release of a constant volume of dammed-up fluid results in an initial slumping phase (Huppert & Simpson 1980), during which time the head velocity is constant. After the head has travelled a distance about equal to ten times the length of the original dammed region, a wave of depression, reflected from the rear wall of the tank, catches up with it (Simpson 1982). The bulbous headwave form disappears, and often a phase of self-similar inertial–buoyancy balance follows, in contrast with the non-similar local control at the head characteristic of the initial motion. The motion of this inertial phase can be found by equating the buoyancy force (8) to the inertial force:

$$F_i \propto \rho U^2 h \propto \rho \frac{L^2}{t^2} h \quad \text{so that} \quad U^2 \propto g'h.$$

Under this balance the spreading law becomes

$$L = k_I\{g'\tilde{q}\}^{\frac{1}{3}} t^{\frac{2}{3}}. \tag{24}$$

Then at a transition time given by

$$\left\{\frac{k_0''}{k_I}\right\}^{\frac{15}{2}}\left\{\frac{\tilde{q}^4}{g'^2\nu^3}\right\}^{\frac{1}{7}}$$

(Huppert 1982; Maxworthy 1982) the viscously controlled regime follows (equation (23)).

4. Experimental results

4.1. *Release of a fixed volume of fluid*

We start with one of the most interesting results of the present study, which was obtained for the case of a fingering interface when R_ρ' was close to unity. In figure 3, we show the length L of the intrusion from its initial position (see figure 1) as a

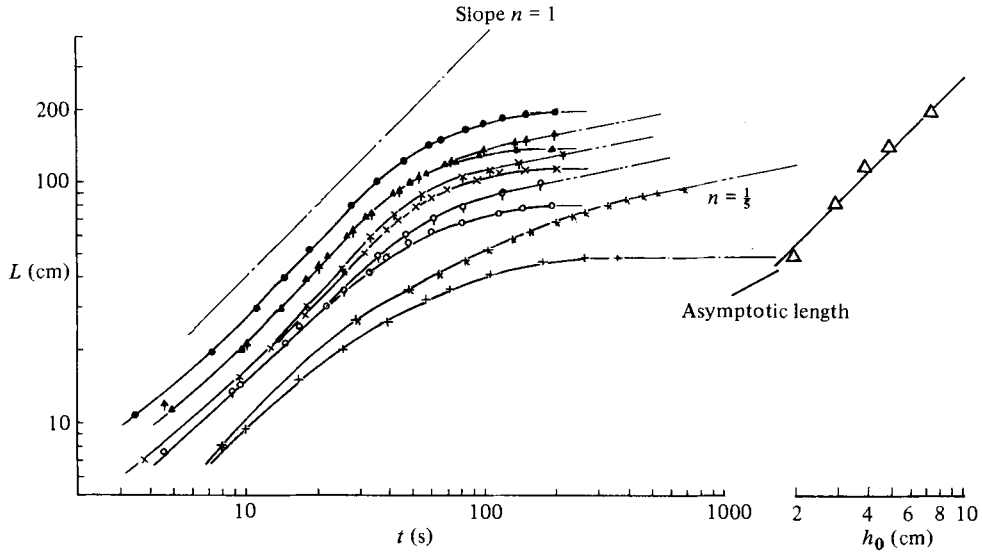

FIGURE 3. Release of a fixed volume of sugar solution of density 1·0425 over a salt solution ($\rho_a = 1{\cdot}045$, $R_\rho = 1{\cdot}06$) to form a fingering interface, and for various values of h_0 (see figure 1). Curves for a non-diffusive interface, salt solution over salt solution, with the same densities are shown for comparison. —●—, $h_0 = 7{\cdot}5$ cm; —▲—, (diffusive, d), —▲— (non-diffusive, nd), $h_0 = 5$ cm; —×— (d), —✳— (nd), $h_0 = 4$ cm; —○— (d), —○— (nd), $h_0 = 3$ cm; —+— (d), —+— (nd), $h_0 = 2$ cm. The asymptotic values of L are also shown as a function of the initial depth h_0; the slope of this line —△— is unity.

function of time t since the withdrawal of the retaining dam. Several effects are immediately apparent. The intrusions with the larger initial volume lengthen rapidly at first, at a constant velocity. However, later in their travel double-diffusive effects become dominant and the intrusions slow and eventually stop! This latter phenomenon is not seen in intrusions for which double-diffusive effects are absent (also plotted in figure 3). Visual observation of these interfaces show several effects which interact to bring about the observed behaviour. Initially the head of the wave looks essentially the same as that for which double diffusion is absent (figure 4(*a–d* or *e*). A small flux of sugar solution can be seen leaving the intrusion, but the high inertia of the flow and perhaps mixing and shear across the interface apparently reduce any important dynamical influence it might have. As the intrusion begins to slow (perhaps after the reflected wave from the endwall catches up to the head (Simpson 1982), but more importantly under the influence of both viscous and double diffusion), the head wave loses its bulbous shape, and convection from the main body of the intrusion becomes intense (figure 4*e* or *f–k*). Ambient fluid is entrained into this falling plume, and ultimately falls to the bottom of the tank and becomes a bottom gravity current, the front of which is indicated by a dotted curve in figure 4 (*k*). Here the double-diffusive configuration is reversed so that fluid with an excess of sugar is riding beneath a brine solution. Under these circumstances a thin 'diffusive' interface is formed, across which further material exchange can take place also. The details of this interesting problem are left until later, when we study the dynamics of this interface in a related experiment. In the present context, the appearance of the secondary gravity current and entrainment into the plume that feeds it is important because the flow induced by these motions interacts with the main intrusion, slows it down and eventually stops it. Diagrammatic details of the flow field are shown in figure 5(*a*). In figure 5(*b*) we speculate that even if the tank were very deep, so that a bottom gravity current could

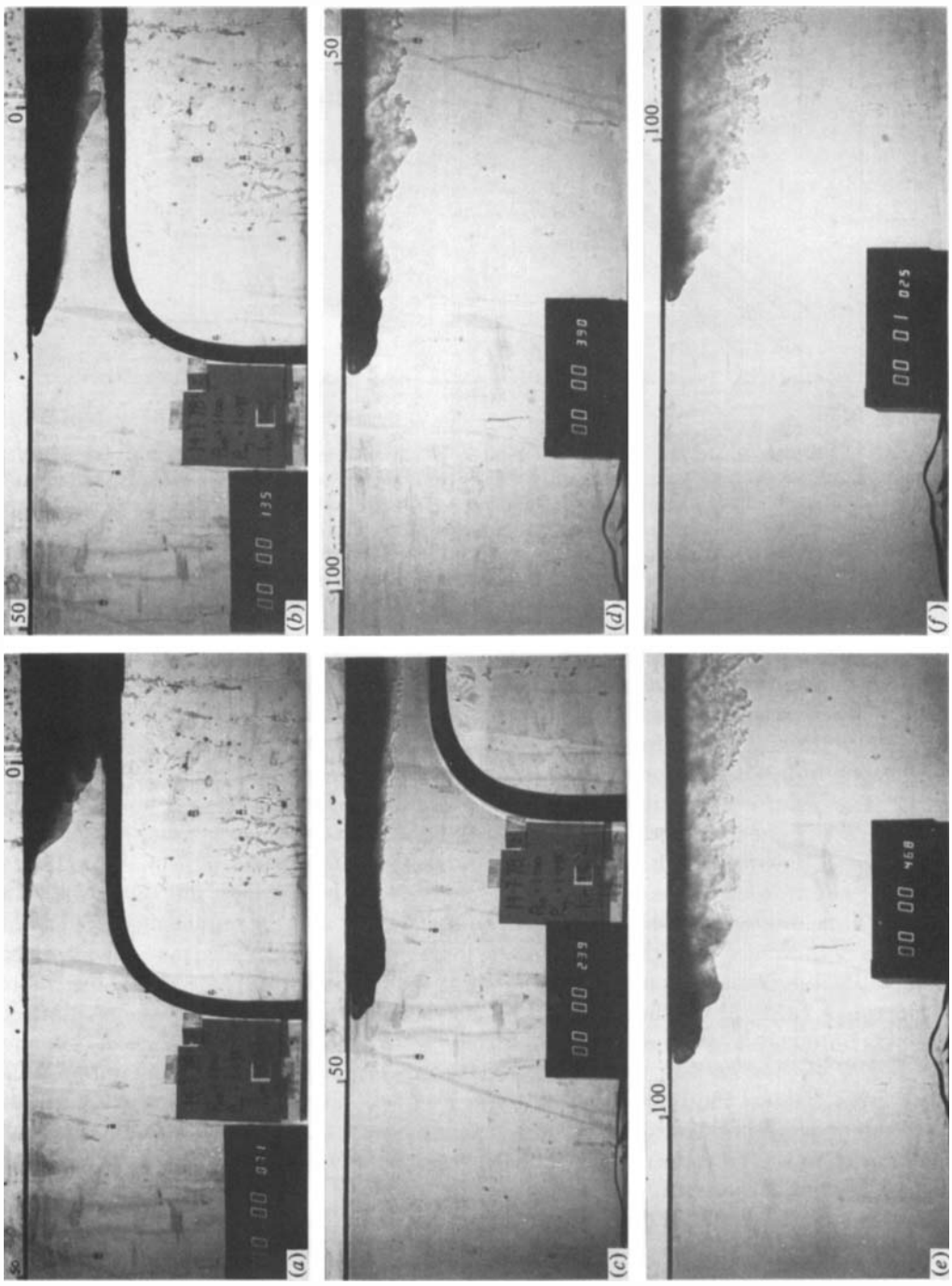
0
50
100
(a)
(b)
(c)
(d)
(e)
(f)

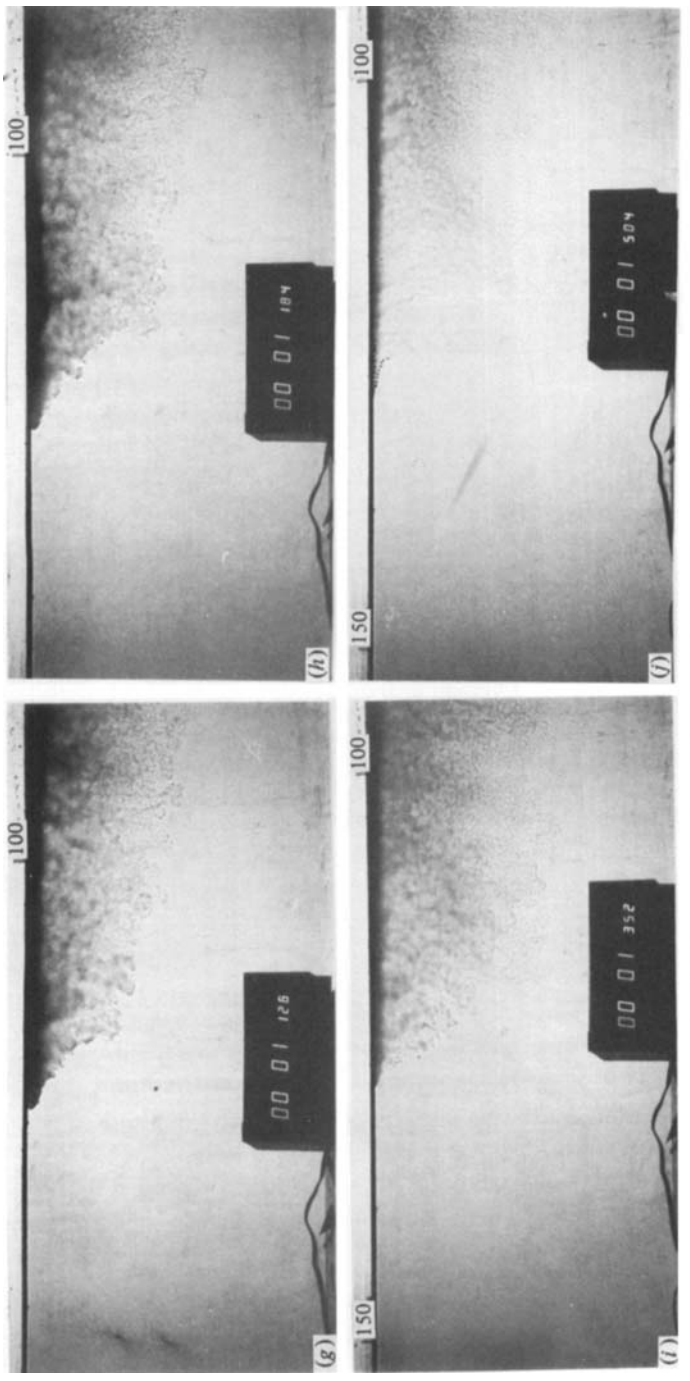

FIGURE 4. Photographs of the progression of states passed through by a constant volume release for the case of a fingering interface. By picture (*h*) the gravity current has stopped. Intense convection is created by loss of heavy sugar solution from the intrusion. A bottom gravity current is formed, indicated by a dotted surface in *k*, the flow over which interacts with the intrusion itself. The nose of the intrusion is also indicated by a dotted line where its location is not well shown in the print. Upper numbers here and in other plates are distance from origin in centimetres.

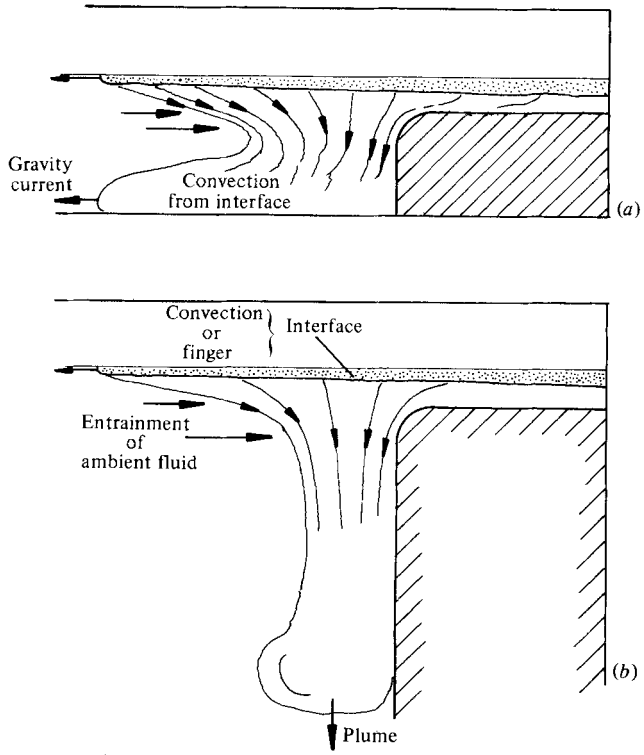

FIGURE 5. (*a*) Diagrammatic view of the formation of a bottom gravity current from the heavy fluid lost from the intrusion. The ambient fluid entrained into this region creates a backwards flow against the general forward motion of the main intrusion. (*b*) Diagram to show how an opposing flow would be formed even in a very deep tank. Entrainment into the downward-moving plume and its feeding jet forms an external flow against the flow of the intrusion.

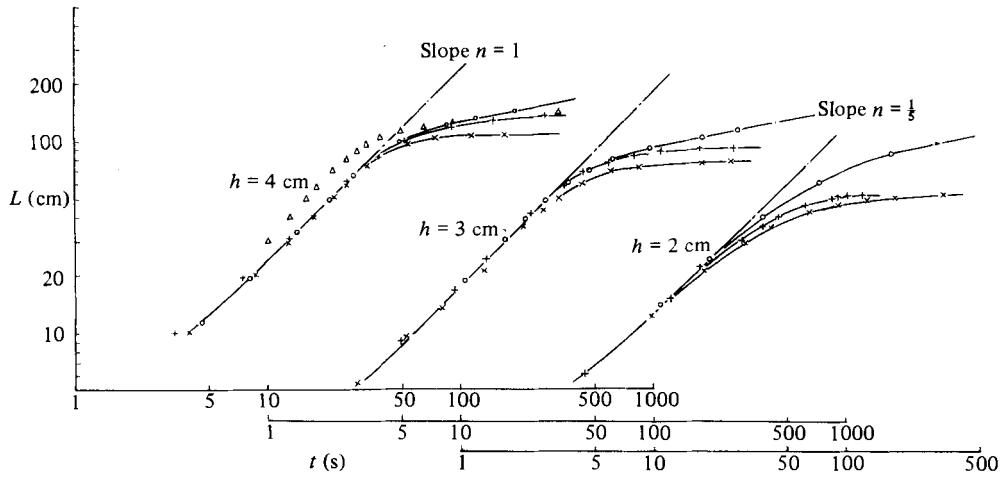

FIGURE 6. Intercomparison of the behaviour of the three types of interface studied: —○—, non-diffusive; —+—, diffusive; —×—, fingering: $\rho_a = 1{\cdot}045$ and $\rho_1 = 1{\cdot}040$ for all except —△—, for which $\rho_a = 1{\cdot}050$ and $\rho_1 = 1{\cdot}040$ and the interface is of the diffusive type. Three values of h_0 are shown: 2, 3, and 4 cm, with staggered abscissae.

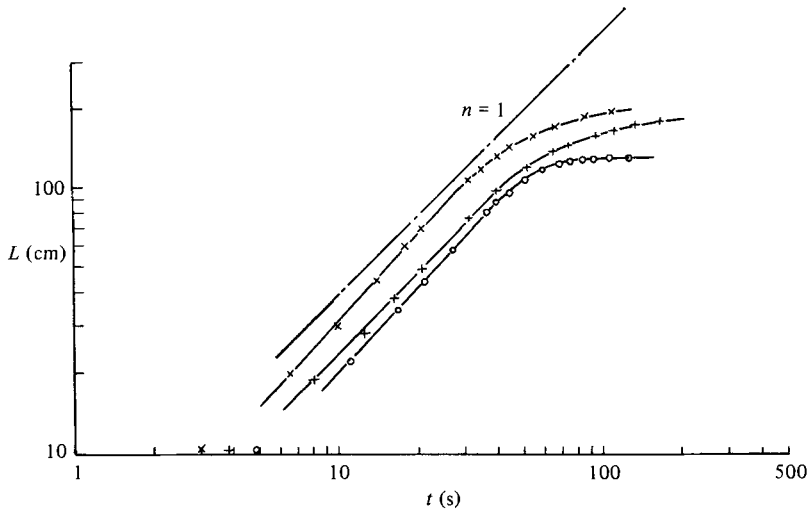

FIGURE 7. Behaviour of a fixed release ($h_0 = 7{\cdot}5$ cm) for a fingering interface and three density ratios: —×—, $\rho_1 = 1{\cdot}040$; —+—, 1·0420; —○—, 1·0425. $\rho_a = 1{\cdot}045$.

not form, entrainment into the jet at the endwall would still create a counter flow to oppose the motion of the surface current.

In the following figures, we compare various different cases in order to show the relative importance of the several effects under our control. In figure 6 we display the relative effects of the three types of interface for a series of otherwise fixed initial conditions. Not unexpectedly, the curves are ordered by the vigour of the convection at the interface, for a given density ratio. The non-diffusive interface eventually travels farther in a given time, followed by the diffusive and finally the 'fingering' interfaces. As discussed in §5, this is presumably the result of the larger convective mass flux that passes through the fingering interface, compared with the amount passing through the diffusive interface for the same density difference.

In figure 7 results for a fingering interface are shown for various density ratios; they are ordered so that the current with the larger initial density difference travels faster. Only in the case of the smallest $\Delta\rho$ does the current actually stop, however, while the other two have not been followed until that state is actually reached, if it ever is. However, in no case have we observed an extended temporal dependence requiring the balance, between interfacial and buoyancy force, described by (17); the flow appears to be quickly dominated by the external velocity field for the range of parameters we have studied in the present experiments.

4.2. *Injection at a constant flow rate*

4.2.1. *Diffusive interface.* Many of the mechanisms controlling the motion of a double-diffusive intrusion can be more clearly seen in this case. We start with a flow rate for which the intrusion always stays well ahead of any bottom current which may form (figure 8). With decreasing R_ρ and hence increasingly vigorous convection, the slopes of the curves decrease from 0·76 to 0·71. Two cases of a non-diffusive interface, i.e. brine over a heavier brine solution, are shown for comparison, while numerous other comparisons can be found in DM and Maxworthy (1982). It appears that the motion of the slug is governed from the very beginning by the stress at the double-diffusive interface, i.e. any transition time is less than one second or so.

In figure 9 the upper curve for the case of at least vigorous convection again

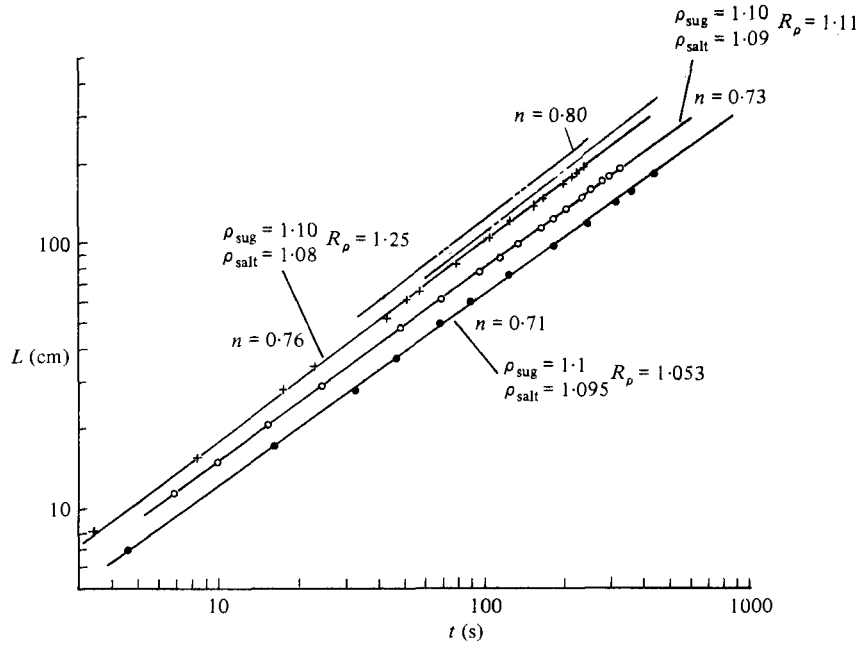

FIGURE 8. Intrusion with a constant inflow. Results are plotted for three values of R_ρ, showing the decrease in slope as the vigour of the convection from the diffusive interface (salt over sugar solution) increases. No distinct bottom gravity current is formed in these cases. The chain-dotted lines —··— and —·— give the predictions of Huppert's (1982) viscous theory for the upper two cases, —+— and —○—. $\tilde{q}$ = 0·74 cm²/s for all cases.

conforms to the results shown in figure 8, even though the flow rate is lower. In the next-lower curve, convection produces a bottom current which just catches up with the leading edge of the intrusion by the time it has reached the end of the tank. The third-lower curve, at the same flow rate but with R_ρ closer to unity, shows a small but distinct increase in slope as the head of the gravity current passes that location, followed by a very rapid increase when it interacts with a reflected wave which is moving back along the newly formed interface and which was created by the reflection of the gravity current from the endwall of the tank. The point is further emphasized in the lowest curve, for an even smaller flow rate, where three distinct slopes are found: n = 0·65 before the gravity-current head reaches the leading edge of the intrusion, 0·71 after, followed by 0·9 upon interaction with the reflected wave. These processes are shown diagrammatically in figure 10 and photographically, for the more dramatic fingering interface, in figure 11. In the first case (figures 10*a*, 11*a–f*) the advancing bottom current creates a strong backwards flow against the intrusion, slowing it down (see §5). However, this current, upon interacting with the endwall, is reflected as an internal surge, which creates a strong forward flow, which then interacts with the intrusion to force it forward (figures 10*b*, 11*g–j*).

Finally, in figure 12 we show data on what we believe to be, after much deliberation, a transition from a current controlled by momentum loss from the intrusion to one controlled by momentum transfer from the ambient, a U-to-U_∞ transition. The corresponding viscous solutions are shown on the figure as chain-dotted lines, and they are well above the corresponding interfacial-stress-controlled curves, as is also the case in figure 8 and 9, while a break to a slope of 0·67 is quite clear. Further discussion of this result is left to §5.

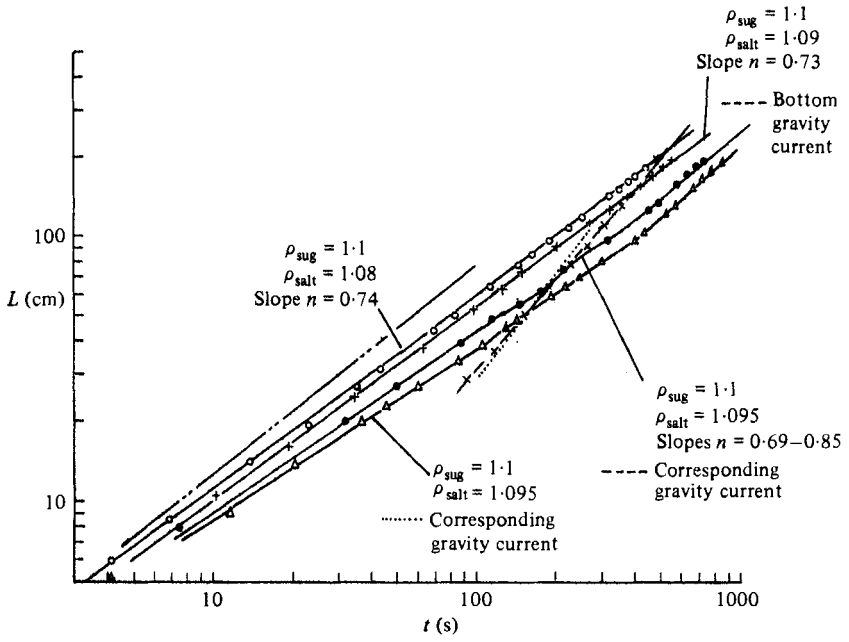

FIGURE 9. A series of cases at lower flow rates for the diffusive interface, and showing the increased importance of interaction with the bottom gravity current as R_ρ becomes closer to unity. Coincidentally, the trajectories of the bottom current for the two cases —●— and —△— were virtually identical and are shown here as one line, ----. For the lower curve —△— three regions can be distinguished. The first, with $n = 0{\cdot}65$, occurs before the bottom current reaches the front of the intrusion; the second, $n = 0{\cdot}71$, occurs after this time, and the third, $n = 0{\cdot}9$, is formed by interaction with a wave on the bottom current formed by reflection of the current head from the endwall. The chain-dotted line gives the prediction of the viscous theory for the uppermost case. $\tilde{q} = 0{\cdot}38$ cm^2/s for all cases except the lower one, for which $\tilde{q} = 0{\cdot}31$ cm^2/s.

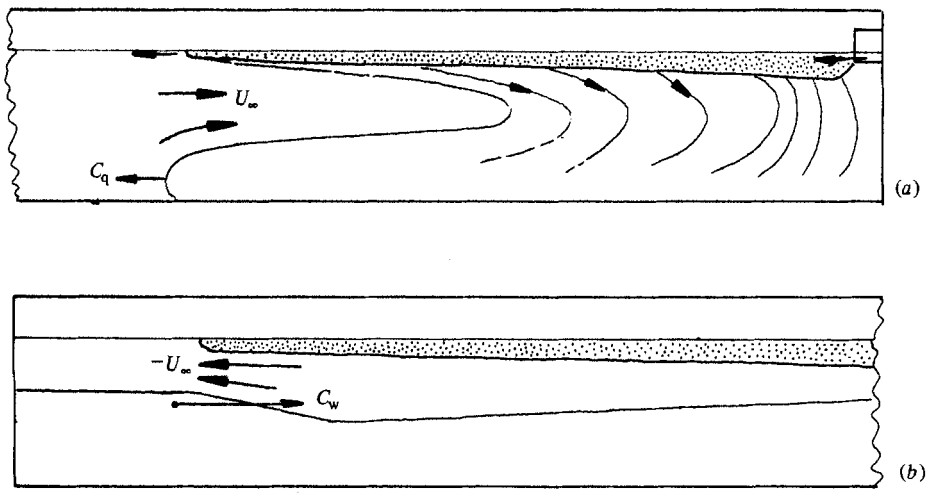

FIGURE 10. Diagrammatic view of the two main phases of flow due to interaction with the bottom current. (*a*) Interaction with flow in the neighbourhood of the head, in which case U_∞ is an increasing function of time. (*b*) Interaction with the reflected wave, in which case the external flow is reversed.

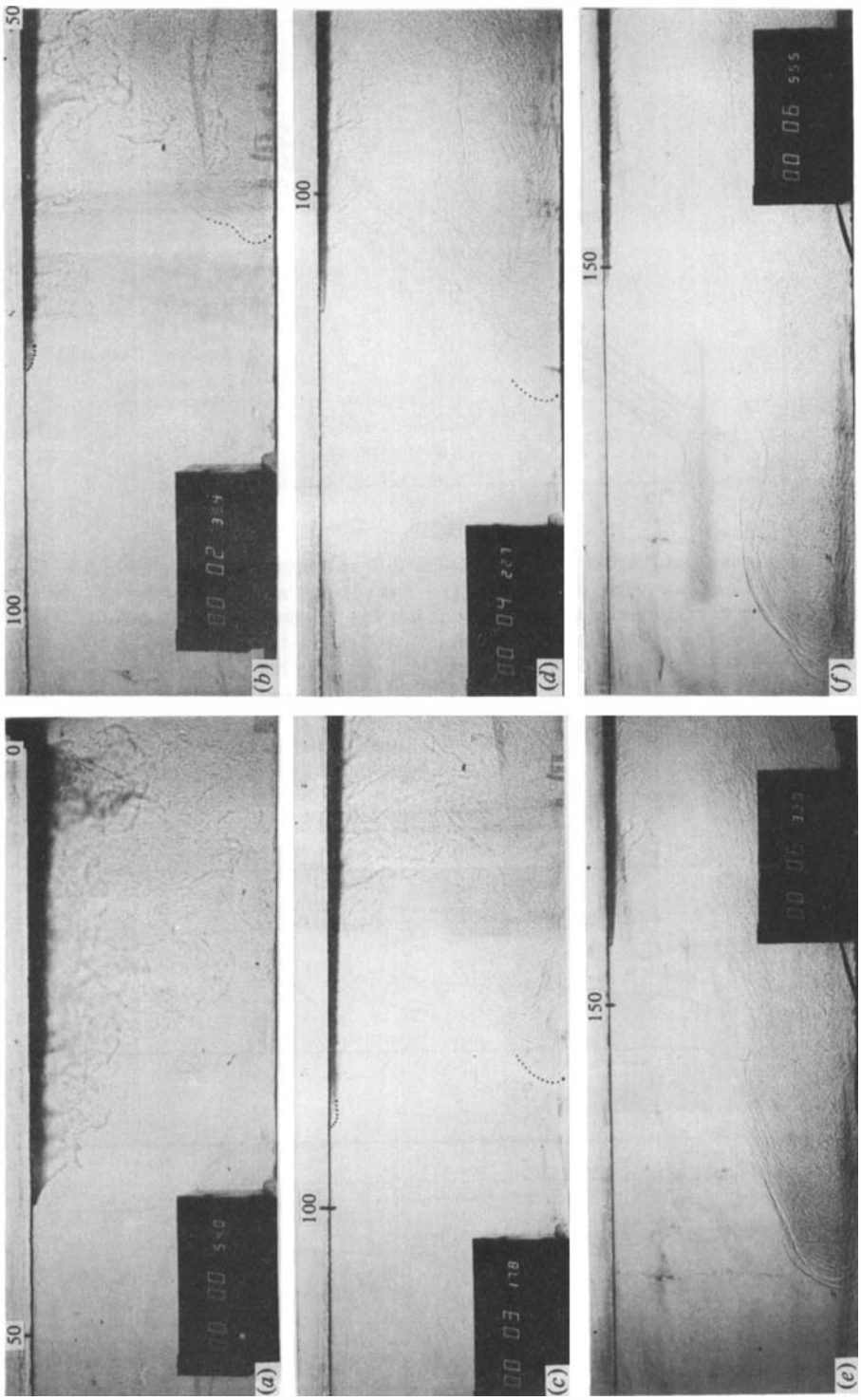
0
50
100
150
(a)
(b)
(c)
(d)
(e)
(f)

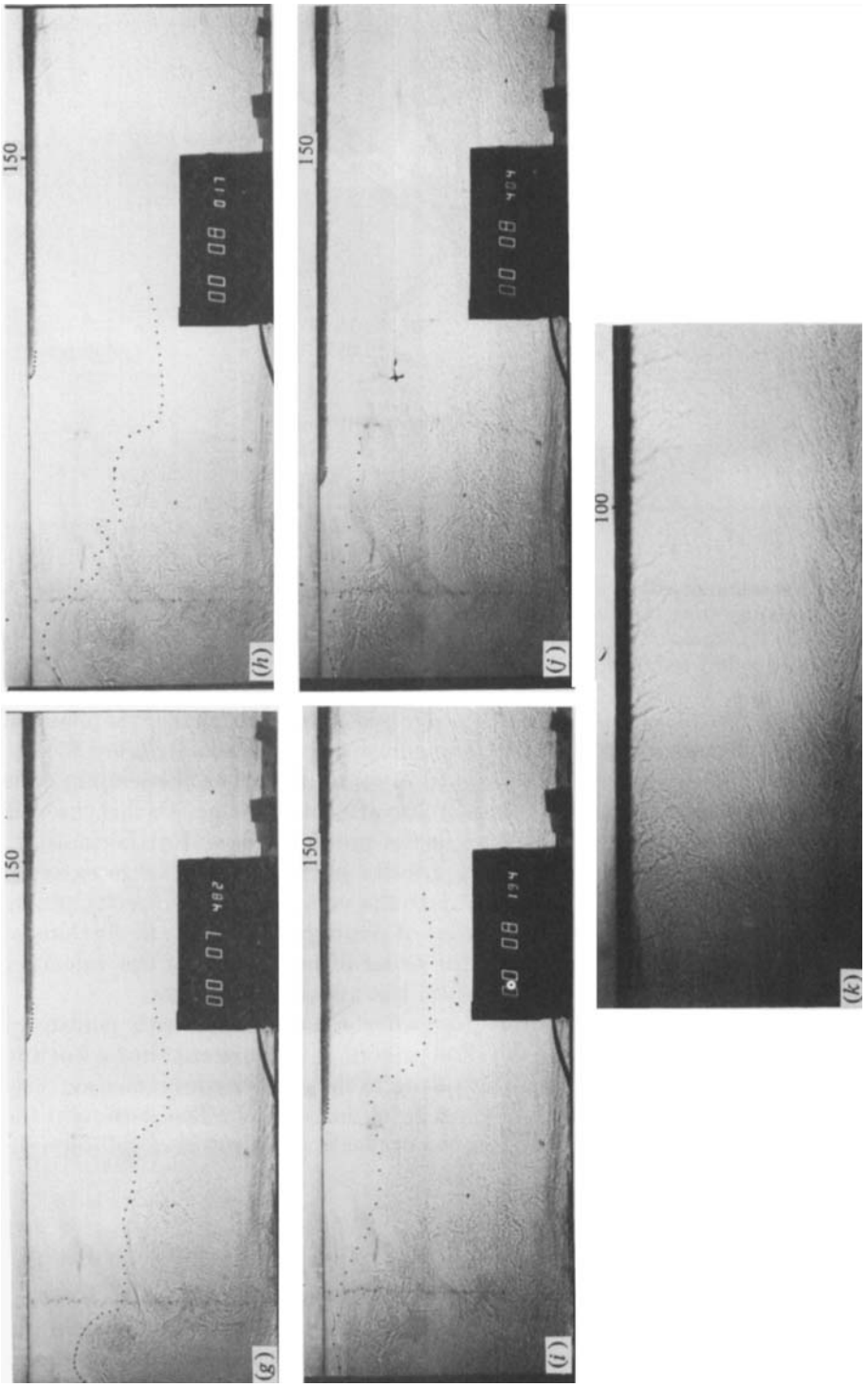

FIGURE 11. Photographs of the interactions shown in figure 10 for a 'fingering' interface. In (*b*) the bottom gravity current begins to form (its nose is indicated by a dotted line in (*b*), (*c*) and (*d*)). In (*g*) the nose interacts with the endwall of the tank to produce a backward-moving wave, (*g*)–(*j*). In (*k*) we show a photograph of the flow after some time, with clear evidence of a bottom flow from right to left and one in the opposite direction just below the upper current.

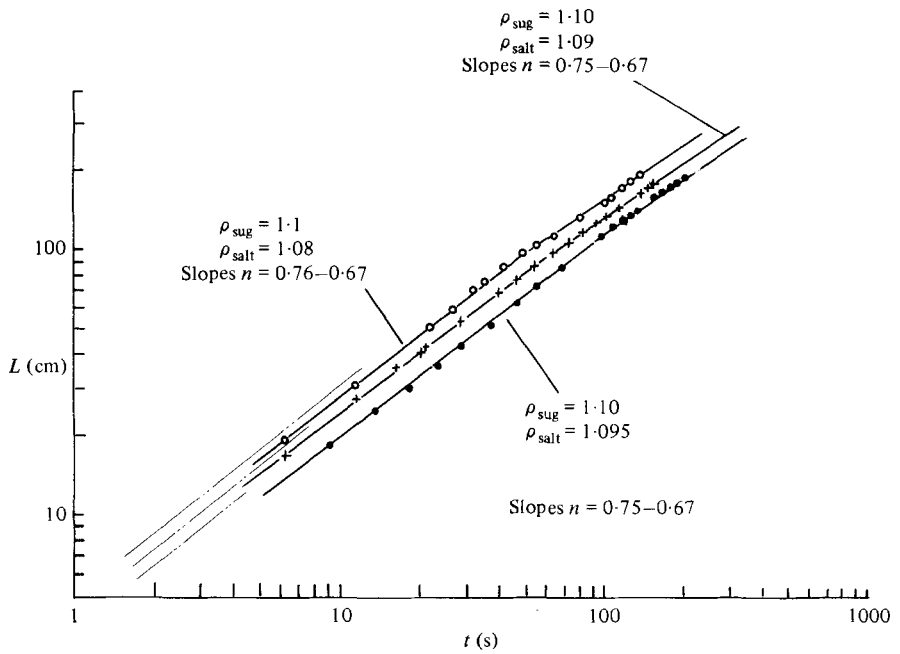

FIGURE 12. Largest value of inflow rate showing a probable transition from intrusion controlled by momentum exchange from the slug (U) to one controlled by momentum interchange from the external flow (U_∞). The chain-dotted lines give the predictions of the viscous theory for all three cases sequentially. $\tilde{q}$ = 1·57 cm^2/s for all cases.

4.2.2. *Fingering interface.* Most of the points raised above are further emphasized when considering the more vigorously convecting fingering interface. In figure 13 note a very small slope before the head of the bottom current reaches the leading edge of the intrusion, followed by a more rapid increase after its passage. In this case the bottom current is much more distinct than in the previous cases. Furthermore, in figure 14 the intrusion outruns the bottom gravity current, but a large external velocity U_∞ is still produced by entrainment into the very intense convective plume that is formed. In figure 15 we present a series of photographs of the distortions of a dye streak, which indicates very clearly the order of magnitude of the velocities and shears being impressed upon the motion of the upper surface flow.

Finally, we show in figure 11(k) the flow after a long time, with continued injection. From the distortions of streaks shown there, it is apparent that a bottom flow from right to left still persists, probably owing to the greater convective activity near the injector, where fresh sugar solution is being introduced. The motion in the outer fluid, close to the upper surface, is in the opposite direction and still opposes the motion of the primary intrusion.

5. Discussion

In §4 we have presented a series of experimental curves of intrusion length L versus time t under a variety of circumstances: for two types of release (constant volume and constant inflow rate) and three possible types of interface between the intrusion and its surroundings. Based on flow-visualization studies, we have found that a flow is formed in the main body of fluid by vigorous convection from two of these interface types. This flow, external to the main current, has a profound effect on its motion.

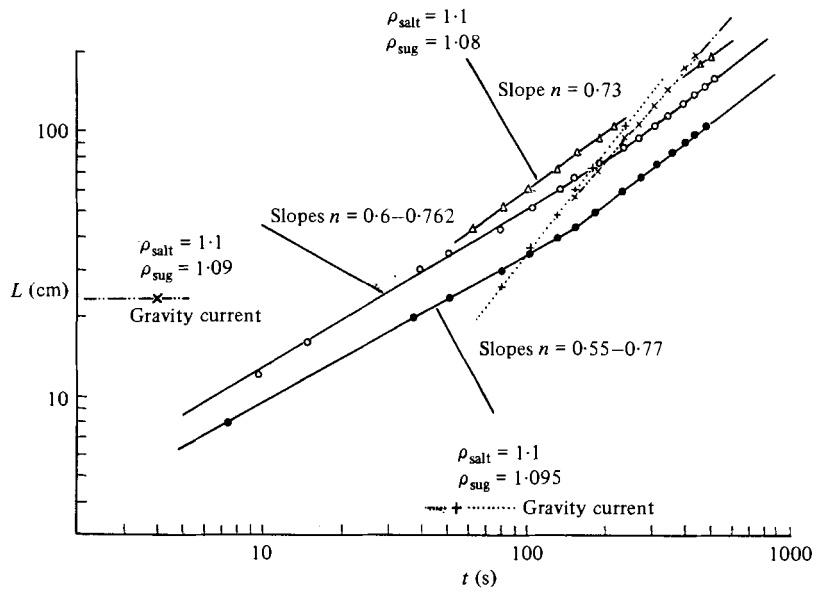

FIGURE 13. Low flow rate for a fingering interface, showing the change in slope as the head of the gravity current passes the front of the wave, —○— and —●—. In the case —△— convection is weak enough that no clear current is formed. $\tilde{q} = 0{\cdot}38$ cm^2/s.

In what follows, we attempt to rationalize all of these results into one more-or-less coherent framework, making use of some of the ideas introduced in §3. The one unfortunate condition that makes detailed numerical comparisons very difficult is the fact that one of the main variables we require, namely the external flow velocity U_∞, is itself a dependent variable, and its relationship to the fixed external variables has not been measured and is unknown. From what we have already seen, it depends strongly on the geometry of the container, and at the moment we have only qualitative ideas about its dependence on the independent parameters of the problem.

Despite this qualification, it is satisfying that the model result presented in (19) predicts that the intrusion should reach a constant fixed length (figure 3) under the circumstances required of that theory. These asymptotic lengths do not scale as $\tilde{q}^{\frac{2}{3}}$ as predicted, possibly because U_∞ is also a function of $\tilde{q}$. Equation (8) suggests it should be $U_\infty \propto \tilde{q}^{-1}$ to agree with the results of figure 3. However, several difficulties cloud this deceptively simple explanation – it is unlikely that any of the quantities assumed to be constant in the right-hand side of (8) will, in fact, be so during the course of any one experiment, since g' is increasing while V and $\tilde{q}$ are decreasing with time. Material is lost from and gained by the intrusion, in such a way that the whole system tends to stratify more strongly (Griffiths & Ruddick 1980; Turner 1973; MacDougall 1982). This increases the driving density difference $\Delta\rho$. At the same time, the density difference driving the convection is being reduced by loss of sugar/salt from the intrusion and its gain of salt/sugar; as a result V not only decreases, but also becomes a function of distance along the intrusion (MacDougall 1982). For the small changes associated with the timespan of interest here, these two effects may be so small that they have no effect on the slug development, although subtle effects can be seen in the constant-flow-rate experiments discussed later.

Unfortunately, the experiments were not run for a long enough time to decide whether the lengths remained constant as the system ran down further. Such a possibility seems remote, since it would also require U_∞ to remain constant, and it

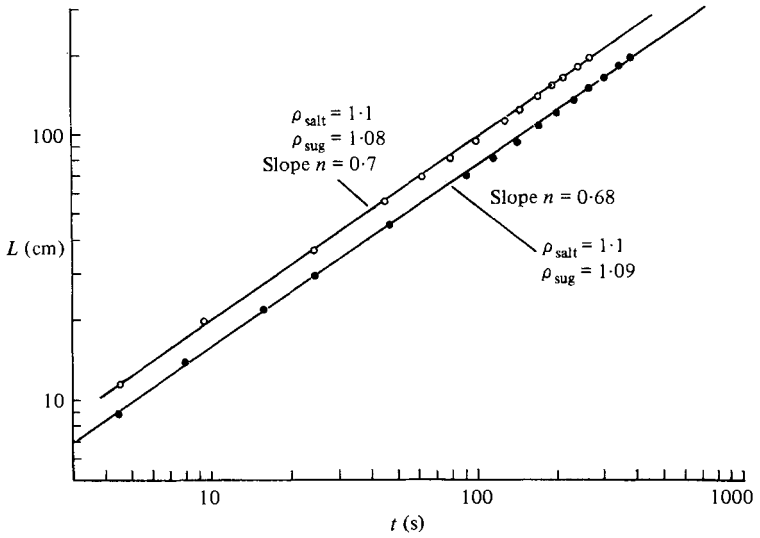

FIGURE 14. L versus t for the more vigorously convective fingering interface. At a moderate flow rate, such that the gravity current is always well behind the front of the intrusion. $\tilde{q} = 0{\cdot}74$ cm^2/s.

seems that it too should decrease as the convection is reduced. This suggests that the constant lengths found in our experiments are a transient phase of a longer-term evolution in which the intrusion eventually spreads the whole length of the tank over a larger timescale.

The results shown in figure 6 and 7 are also consistent with this basic idea, with the more vigorously convecting systems, i.e. large V, tending to produce shorter slug lengths. Also, in no case do we see an extensive region of slug-dominated interfacial stress represented by the power-law behaviour $t^{\frac{1}{2}}$, (17), suggesting that if it exists it is only a transitory phase between the inertial, head-controlled, constant-velocity regime and one dominated by the external flow. All of this, plus the fact that U_∞ is also a function of time during the transition to a constant length, makes it impossible at this stage to test either of the estimates (18) and (20) of transition time from one regime to another.

The results found for the case of a constant inflow ($\alpha = 1$) are more useful in unravelling some of the problems with which we are still faced. At moderate flow rates and for a diffusive interface (figure 8) for which the bottom gravity current is not an important factor, the slope of the L versus t lines are reassuringly close to that predicted in (13), when the convection is the least vigorous (upper curve and possibly the next lower). As the magnitude of the convection increases, this slope is reduced. Since the flow apparently still remains similar, reflected in the fact that the evolution can be described by a power law, it is unlikely that we are seeing the effect of the outer flow, since this is an additive effect not a multiplicative one. We suggest, based on the experimental observation of a large volume flux from the intrusion (figure 11), that this decrease in slope is due to an effective value of $\tilde{q}$ which is also a decreasing function of time and not a constant as assumed. To rationalize this comment one can show that the difference between the downward velocity V_D and the upward velocity V_U at a salt–sugar interface is given by

$$V_D - V_U = \frac{6{\cdot}3 \times 10^{-3}}{\rho} (\alpha \Delta T)^{\frac{1}{3}} R_\rho^{-12{\cdot}6} \left\{1 - R_f \frac{\alpha \Delta T}{\beta \Delta S}\right\}$$

for the diffusive interface, as an example, where R_f is the flux ratio, which has an

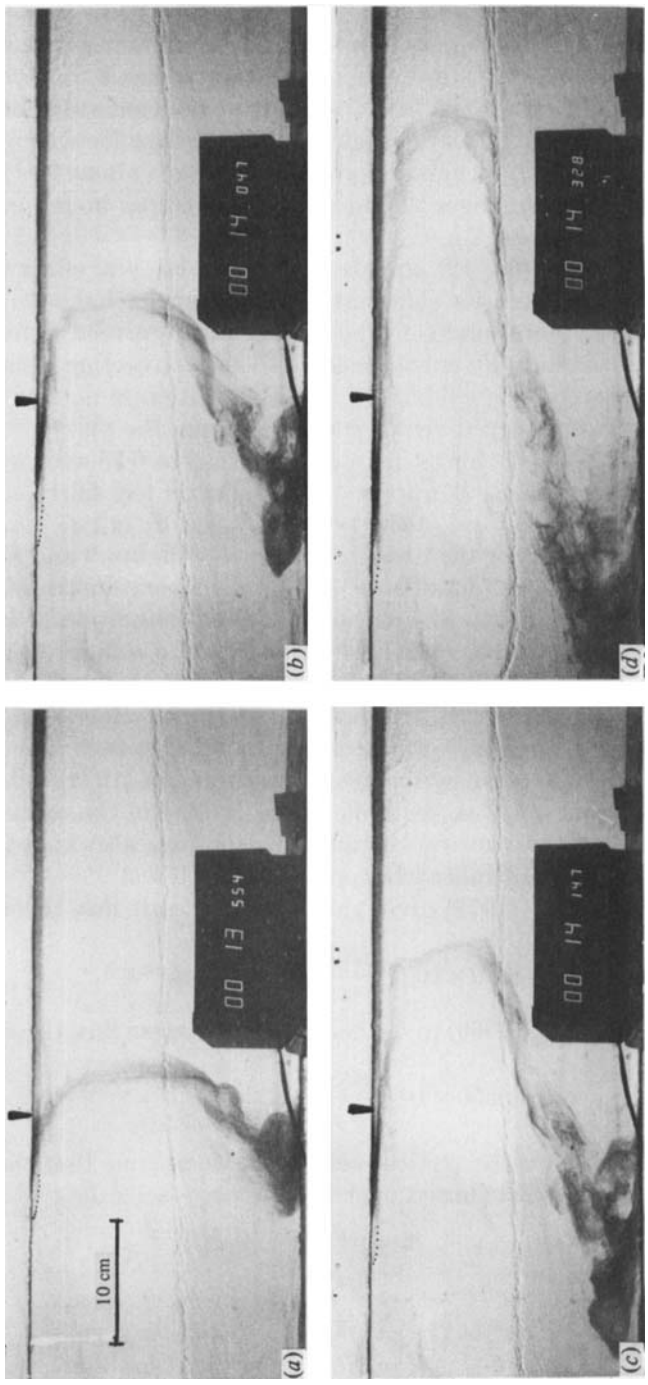

FIGURE 15. Distortions of an initially straight dye streak introduced at the location indicated by the arrow head at 13:45·9 on the clock. The diffusive interface between the bottom current and the original salt solution is very clear as is the large external velocity U_∞ being impressed upon the intruding layer of sugar solution. The poorly reproduced nose of this layer is shown by a dotted line in each photograph. Note indications of a returning wave at the left of (*d*).

almost constant value of 0·6 in this case (Shirtcliffe 1973). This velocity difference is positive for all cases considered here, so that there is a net loss of volume from the intrusion as time progresses, as already noted. This loss is further enhanced by the increase in slug length with time, which increases the area over which material transport can take place. At the same time g' is slowly increasing and V decreasing, but we suggest, based on (13), that the loss of volume more than compensates for this and causes the effective slope to be below the predicted value of $\frac{3}{4}$. Only at the largest value of R_ρ or when $\tilde{q}$ is large (figure 12) are these effects small, and we then obtain close agreement with the prediction, otherwise the volume loss is an important effect and the theory is no longer valid except as an upper bound on the observed behaviour.

At higher flow rates (figure 12), apparently we see the real effect of the external flow, a transition from a intrusion-dominated momentum exchange to one dominated by the external flow. Here again, no bottom gravity current is formed, and the external flow is caused only by entrainment into the convecting plume beneath the intrusion. Unfortunately, the evidence for this transition is not strong, because of the experimental error involved in determining L from the photographs. However, the facts that the measured curves have a slope close to 0·75 and are substantially below the viscous predictions (Huppert 1982) make us feel fairly certain that the initial portions of the curves are of the type described by (13).

In these cases (and also for the two upper curves of figure 9 and the upper curve of figure 13, discussed in more detail later) we have sufficient information to estimate values for k_1, (13), and C_1, (14). As mentioned before, estimation of k_1, (15), and C_1', (16), requires a knowledge of U_∞ which we do not have to sufficient precision, except to say that is of the order of 1 cm/s in many of the cases considered. We use the flux laws measured by Shirtcliffe (1973) for the diffusive interface and by Griffiths & Ruddick (1980) for the fingering interface to estimate V in each case. We ignore the effect of shear on these fluxes, as documented by Linden (1974), although it could be an important effect which causes some of the scatter in the calculated values of k_1. Since all of the other quantities in the equations are also known, we can then calculate values for the multiplicative constants of interest.

In summary, Shirtcliffe (1973) gives the downward salt flux through a diffusive interface as

$$F_{\mathrm{t}} = 6{\cdot}30 \times 10^{-3} \frac{(\alpha \Delta T)^{\frac{4}{3}}}{\alpha} R_\rho^{-12{\cdot}6} \text{ g cm}^{-2} \text{ s}^{-1}, \tag{25}$$

while Griffiths & Ruddick (1980) give the downward sugar flux through a fingering interface as

$$F_{\mathrm{S}} = 5{\cdot}50 \times 10^{-3} \frac{(\beta \Delta S)^{\frac{4}{3}}}{\beta} R_\rho^{-6} \text{ g cm}^{-2} \text{ s}^{-1}. \tag{26}$$

For simplicity, to estimate the vertical velocity V we assume that the flux given by (25) or (26) is uniformly distributed over the interface according to the formula

$$\begin{aligned} F_{\mathrm{I}} &= \rho V \Delta I \\ &\equiv \frac{\rho V}{\gamma} (\gamma \Delta I), \end{aligned}$$

where I is either T or S, and γ is α or β respectively. Combining this with (25) or (26) gives for the diffusive interface

$$V = \frac{6{\cdot}30 \times 10^{-3}}{\rho} (\alpha \Delta T)^{\frac{1}{3}} R_\rho^{-12{\cdot}6} \text{ cm/s}, \tag{27}$$

and for the fingering interface

$$V = \frac{5{\cdot}50 \times 10^{-3}}{\rho} (\beta \Delta S)^{\frac{1}{3}} R_\rho^{-6} \text{ cm/s}. \tag{28}$$

These estimates for V are shown in table 2, and, when combined into (13) and (14), give the estimates for k_1 and $C_1 = (k_1/k_v)^{20}$; these are also shown in table 2, together with the calculated values of t_{TR}.

	$V \times 10^4$ cm/s	k_1	$C_1 \times 10^{12}$	t_{TR} (s)
Figure 8, case 1*a*	1·03	0·18	0·1	3
1*b*	3·64	0·23	13·5	0·4
Figure 9, case 2*a*	1·03	0·15	0·0026	0·3
2*b*	3·64	0·21	2·18	0·2
Figure 12, case 3*a*	1·03	0·18	0·1	0·7
3*b*	3·64	0·24	31·5	0·2
3*c*	5·62	0·26	156	0·05
Figure 13, case 4	3·91	0·21	2·18	0·02
Average values, $\bar{k}_1 = 0{\cdot}21$, $\bar{C}_1 = 2{\cdot}18 \times 10^{-12}$				

TABLE 2

In view of similar results found for gravity currents with variable inflow (Maxworthy 1982), it is not surprising that the values of C_1 are so small and so scattered. This reflects the fact that the coefficient k_1 is somewhat smaller than one might at first believe based on the usual expectation that such quantities should be of order unity in order-of-magnitude calculations such as these. Because the slopes of the two curves are so closely matched (0·8 compared with 0·75) small variations in k_1 make enormous differences in the transition time, as reflected in the fact that C_1 is the ratio k_1/k_v raised to the power 20.

Unlike the situation in Maxworthy (1982), where we knew all of the independent variables precisely, in the present case our estimate of V might be cause for some concern. For example, a measurement error in the density of only 0·3 % for any of the solutions results in, typically, a 60 % error in the value of V and a corresponding error of 13 % in k_1, easily sufficient to explain the variations in k_1 found in table 2. At the moment the value of $\bar{k}_1 = 0{\cdot}21$ is the best estimate for the quantity until more accurate and complete experiments are performed in the future. As in Maxworthy (1982) the possibility arises that, although the flow during any one experiment remained similar, the coefficients of proportionality in (4), (5) and (8) may in fact vary from experiment to experiment, owing, among other things, to increased mixing at the higher flow rates. Resolution of such a question requires detailed measurements of velocity and density distribution within the flow, which are beyond the scope of the present simple experiments. Similarly, the use of the results of figure 12 to calculate values of k_1 and C_1 is difficult without a knowledge of the variation of U_∞ with the independent variables, and this calculation too must await a more complete experimental investigation.

It is at the lower flow rates (figure 9) that we begin to see the dramatic effects of the bottom gravity current. In the lower two curves the initial slope is small and close

to $\frac{2}{3}$ by the suggesting control outer flow, (15). This condition is even more strongly in evidence for the fingering interface (figure 13). In fact in this latter case, the slope is substantially below the value of $\frac{2}{3}$ predicted by our simple model. We suggest that, as in the case of the diffusive interface, this is likely to be due to a time-dependent decrease in the total volume of fluid in the intrusion, and hence a $\tilde{q}$ that is a decreasing function of time, the effect of which overwhelms the opposing changes in g', V and possibly U_∞, (15). The subsequent increase in slope after passage of the bottom, secondary gravity current is harder to explain, since the outer flow U_∞ must increase in magnitude owing to flow over the gravity current. This process is shown diagrammatically in figure 10(*a*) and photographically in figures 11(*a–f*). One possibility is that the passage of the bottom current changes the pressure field at the bottom of the intrusion, tending to squeeze and thin it; this in turn would cause an increase in its velocity, and hence increase the slope of the L versus t curve. This result can be most readily seen by noting that the increase in external velocity at the bottom of the intrusion, caused by gravity-current passage, would produce a decrease in pressure. Hydrostatic balance within the intrusion requires that it become thinner to accommodate this pressure decrease.

Thereafter, the nose of the bottom gravity current interacts with the endwall of the tank and is reflected along the newly formed interface as an internal hydraulic jump. This jump travels back along the tank and interferes further with the slowly advancing intrusion. Now, however, U_∞ has changed direction in the flow over this wave, so that the external flow now not only accelerates the motion of the intrusion (figures 10*b*, 11*g–j*) but also squeezes it further, and the slope is even larger than that for a viscously controlled current (lower two curves of figure 9). In the case of the fingering interface (lower two curves of figure 13), this latter interaction took place after the completion of the experiment and was not recorded. For both types of interface (upper two curves of figure 9 and upper curve of figure 13) the less-active interfaces propagate with slopes close to the value of $\frac{3}{4}$ predicted in §3. Finally, the fingering interface at a moderate flow rate (figure 14) conforms to the idea that the net loss of intrusion volume is responsible for the decreased slope.

6. Conclusions

We have measured the spreading rates of two-dimensional double-diffusive intrusions, considering both 'fingering' and 'diffusive' interfaces and two types of fluid release, a constant volume and constant flow rate. In all cases considered, the transfer of mass and momentum across the interface quickly dominates the motion of the intrusion, and under suitable circumstances simple order-of-magnitude arguments can be used to develop equations that describe the motion of the leading edge of the intrusion with reasonable accuracy under some circumstances. The major unknown factor is the magnitude of the external velocity imposed upon the layer by entrainment into the convective plume beneath the intrusion. In a relatively shallow tank, such as ours, this convective plume can also, under some circumstances, create a secondary, bottom gravity current, and the flow created by the motion of the latter can also interact with the main intrusion and affect its motion in a manner that, although it cannot be modelled at present, can be understood qualitatively and in a way that gives hope for a suitable model in the future.

The work reported here was performed while I was visiting the Research School of Earth Sciences, Australian National University, Canberra, as the guest of Professor

J. Stewart Turner, F.R.S. I wish to thank him for providing such stimulating surroundings and for making my stay such a pleasant one, both scientifically and personally. I would also like to thank Ross Wylde-Brown and Derek Corrigan for their able technical assistance. Dr Herbert Huppert in his critical review of the manuscript made numerous valuable suggestions, while I drew heavily upon his work on viscous gravity currents in order to improve the presentation of the order of magnitude models; his conscientious effort is greatly appreciated.

The work was partially supported at University of Southern California by the Office of Naval Research under Contract no. N00014-82-K-0084.

Appendix. Axisymmetric double-diffusive gravity currents

For the sake of completeness and because of its likely importance in natural and technological flows, we present here results for the axisymmetric current. In this case equation 4 for the interfacial stress when the intrusion momentum is dominant becomes†

$$F \propto \rho U V R^2, \tag{A 4}$$

and we assume

$$hR^2 \propto \tilde{Q} t^{\beta}, \tag{A 5}$$

where R is the radius of the current and $U = R/t$. Also

$$F_{\mathrm{g}} \propto \Delta\rho g h^2 R, \tag{A 8}$$

while the viscous current behaves as

$$R = k'_{\mathrm{VA}} \left\{\frac{g'\tilde{Q}^2}{\nu}\right\}^{\frac{1}{8}} t^{(3\beta+1)/8} \tag{A 6}$$

(Huppert 1982). Hence an intrusion (U)-dominated current will spread as

$$R = k_{\beta} \left\{\frac{g'Q^2}{V}\right\}^{\frac{1}{6}} t^{(2\beta+1)/6}, \tag{A 9}$$

with a transition time from or to a viscous–buoyancy balance given by

$$t_{\mathrm{TR}} = \left\{\frac{k'_{\mathrm{VA}}}{k_{\beta}}\right\}^{24/(1-\beta)} \left\{\frac{\tilde{Q}V^4}{\nu^3 g}\right\}^{1/(1-\beta)}. \tag{A 7b}$$

On the other hand, an intrusion dominated by the external flow U_{∞} will spread like‡

$$R = k'_{\beta} \left\{\frac{g'\tilde{Q}^2}{U_{\infty} V}\right\}^{\frac{1}{5}} t^{2\beta/5}, \tag{A 10}$$

with a transition time given by

$$t_{\mathrm{TR}} = \left\{\frac{k'_{\mathrm{VA}}}{k_{\beta}}\right\}^{40/(5-\beta)} \left\{\frac{U_{\infty}^8 V^8}{\nu^5 Q g'^3}\right\}^{1/(5-\beta)}. \tag{A 11}$$

For the U-to-U_{∞} transition the time is given by

$$t_{\mathrm{TR}} = \left\{\frac{k_{\beta}}{k'_{\beta}}\right\}^{30/(2\beta-5)} \left\{\frac{U_{\infty}^6 V}{g'\tilde{Q}^2}\right\}^{1/(2\beta-5)} \tag{A 12}$$

† Equation numbers correspond to those given in the text for the plane current.

‡ Note that the current length again becomes constant when $\beta = 0$.

REFERENCES

DIDDEN, N. & MAXWORTHY, T. 1982 The viscous spreading of plane and axisymmetric gravity currents. *J. Fluid Mech.* **121**, 27–42.

FISCHER, H. B. 1971 The dilution of an undersea sewage cloud by salt fingers. *Water Res.* **5**, 909–915.

GRIFFITHS, R. W. & RUDDICK, B. R. 1980 Accurate fluxes across a salt–sugar finger interface deduced from direct density measurements. *J. Fluid Mech.* **99**, 85–95.

HOULT, D. P. 1972 Oil spreading on the sea. *Ann. Rev. Fluid Mech.* **4**, 341–368.

HUPPERT, H. E. 1982 The propagation of two-dimensional and axisymmetric viscous gravity currents over a rigid horizontal surface. *J. Fluid Mech.* **121**, 43–58.

HUPPERT, H. E. & SIMPSON, J. E. 1980 The slumping of gravity currents. *J. Fluid Mech.* **99**, 785–799.

HUPPERT, H. E. & TURNER, J. S. 1981 Double-diffusive convection. *J. Fluid Mech.* **106**, 299–329.

LINDEN, P. E. 1974 Salt fingers in steady flow. *Geophys. Fluid Dyn.* **6**, 1–27.

MACDOUGALL, T. 1982 A model of a frictionless double-diffusive gravity current on a horizontal surface. *Rep. R.E.S., Austr. Natl Univ., Canberra.*

MAXWORTHY, T. 1983 Gravity current with variable inflow. *J. Fluid Mech.* **128**, 247–257.

RUDDICK, B. & TURNER, J. S. 1979 The vertical length scale of double-diffusive intrusions. *Deep-Sea Res.* **26**, 903–913.

SHIRTCLIFFE, T. G. L. 1973 Transport and profile measurements of the diffusive interface in double diffusive convection with similar diffusivities. *J. Fluid Mech.* **57**, 27–43.

SIMPSON, J. S. 1982 Gravity currents in the laboratory, atmosphere and ocean. *Ann. Rev. Fluid Mech.* **14**, 213–234.

STERN, M. E. & TURNER, J. S. 1969 Salt fingers and convecting layers. *Deep-Sea Res.* **16**, 497–511.

TURNER, J. S. 1973 *Buoyancy Effects in Fluids.* Cambridge University Press.

TURNER, J. S. 1974 Double-diffusive phenomena. *Ann. Rev. Fluid Mech.* **6**, 37–56.

TURNER, J. S. 1978 Double-diffusive intrusions into a density gradient. *J. Geophys. Res.* **83**, 2887.